Superconductivity in the transition-metal series

X. Q. Hong and J. E. Hirsch
Department of Physics, University of California, San Diego, La Jolla, California 92093-0319
(Received 20 May 1992; revised manuscript received 13 August 1992)

We study the possibility of describing superconductivity in the transition-metal series within the model of hole superconductivity. The band structures for transition metals are obtained within a tight-binding scheme using the parameters calculated by Papaconstantopoulos, and a rigid-band interpolation scheme is used to describe alloys. bcc, hcp,and fcc structures are considered. Under the assumption that superconductivity originates in the band with closest holelike character to the carriers at the Fermi surface, we obtain parameters in the model that reproduce the experimental values for T_c. The absence of superconductivity at the beginning of the transition-metal series is naturally explained within this model. The possible effect of interband coupling within the model of Suhl *et al.* is also considered. Finally, the nature of the superconducting state and various observable properties are discussed.

I. INTRODUCTION

The explanation of the variations of the superconducting T_c in the transition-metal series is a long-standing problem. Matthias[1] formulated his well-known "rules" many years ago, which postulated that certain values of electron-per-atom (e/a) ratios were particularly favorable for superconductivity. Posterior extensive work[2,3] on a range of alloys of transition metals in different columns and rows in the periodic table established a rather simple and well-defined behavior of T_c vs e/a essentially identical in all three transition-metal series: two bell-shaped curves, peaked approximately at e/a values of 4.7 and 6.5 and width of approximately 1.5 and 2 in e/a values, respectively.

There have been several theoretical attempts to explain this behavior within the generally accepted electron-phonon mechanism of superconductivity. In the early work by Pines,[4] it was argued that the variation in the density of states at the Fermi level $N(0)$ was chiefly responsible for the observed variation of T_c with e/a, through the relation

$$T_c = 1.13\langle\hbar\omega\rangle e^{-1/\lambda} , \tag{1}$$

$$\lambda = N(0)V , \tag{2}$$

with V the effective electron-phonon interaction and $\langle\hbar\omega\rangle$ the average phonon frequency. Posterior work by McMillan[5] and others analyzed in more detail the electron-phonon interaction that enters into V. The dimensionless electron-phonon coupling constant [Eq. (2)] was written as

$$\lambda = \frac{N(0)\langle J^2\rangle}{M\langle\omega^2\rangle} \equiv \frac{\eta}{M\langle\omega^2\rangle} , \tag{3}$$

with $\langle J^2\rangle$ an average over the Fermi surface of the square of a matrix element of the electronic wave function with the gradient of the crystal potential, $\langle\omega^2\rangle$ an averaged squared phonon frequency, and M the ionic mass. It was argued empirically by McMillan that the numerator in Eq. (3), η, is nearly constant in transition metals and that T_c is determined by the denominator in Eq. (3), which gives the "stiffness" of the lattice. Posterior theoretical work by Hopfield[6] attempted to justify this assumption theoretically by calculating η in terms of atomic properties. It should be noted also that in the McMillan equation[5] for T_c, which is a modified form of Eq. (1) that is obtained within Eliashberg theory, the Coulomb pseudopotential μ^* appears, which is difficult to calculate theoretically and is often used as an adjustable parameter.

There have been a number of attempts to compute λ from first principles[7–10] for transition as well as other metals. In addition, other theoretical work estimated λ from some observable property, e.g., resistivity, using a first-principles calculation of the plasma frequency.[11] Generally these works conclude that their predictions for T_c agree with observations.[12] However, there are exceptions, for example, the case of Li.[13] Additionally, as reviewed by Gladstone *et al.*[14] for the transition-metal series, no simple theoretical explanation exists for the absence of superconductivity both at the beginning (Sc,Y) and the end (Pd,Pt) of the series. Also, even using only measured quantities there are sometimes problems in correlating observations with the conventional theory: for example, both in Nb (Ref. 15) as well as in BaPbBiO (Ref. 16), it has been pointed out that the value of λ inferred from the phonon structure in the tunneling density of states is too low to account for the observed T_c. Furthermore, the existence of high-temperature superconductivity in certain oxides[17] is so far unaccounted for within the conventional electron-phonon mechanism. Finally, the empirical observation[18] that a strong correlation exists between the existence of superconductivity in metals and alloys and a positive value of their Hall coefficient, does not have an explanation within the conventional theory at the present time.

One may dismiss the above-mentioned instances as minor exceptions within a theoretical framework that has, for the most part, been overwhelmingly successful.

Alternatively, one may decide that these anomalies, even if not widely recognized as important,[19] warrant exploration of other theoretical approaches to the problem. We adopt the latter point of view in this paper and attempt to describe superconductivity in the transition-metal series within the model of hole superconductivity.[20–22]

In the model of hole superconductivity, pairing originates in an electron-electron interaction term that breaks electron-hole symmetry. This interaction gives rise to superconductivity when the Fermi level is close to the top of a band. Electron-phonon interactions are assumed to be of secondary importance (together with electron-exciton, -plasmon, and other second-order processes) and are neglected in this paper. In Sec. II we give a brief review of this model, and describe the calculational procedure used to obtain the band structures in the transition-metal series. In Sec. III we compute parameters in the model that can reproduce the observed T_c values, and in Sec. IV we evaluate various observables in the superconducting state within our model. We conclude in Sec. V with a summary of results and discussion of their possible relevance to the real materials.

II. THE MODEL AND CALCULATIONAL DETAILS

The basic assumption of the model of hole superconductivity is that Coulomb interactions between carriers in a band cause the effective mass of the carriers to increase as the band filling increases. Then, for the Fermi level close to the top of the band, hole carriers can dynamically lower their effective mass by pairing, as pairing of holes "locally" reduces the band filling. Reduction of effective mass is advantageous at low temperatures due to the resulting gain in kinetic energy.

The pairing interaction in this model is given by[20]

$$V_{kk'}=U-K\left[\frac{\varepsilon_k-\varepsilon_0}{D/2}+\frac{\varepsilon_{k'}-\varepsilon_0}{D/2}\right]+W\left[\frac{\varepsilon_k-\varepsilon_0}{D/2}\right]\left[\frac{\varepsilon_{k'}-\varepsilon_0}{D/2}\right] \tag{4}$$

for a single band. Assuming only nearest neighbor interactions, $W=zV$ with V the nearest neighbor Coulomb repulsion and z the number of nearest neighbors, and $K=2z\Delta t$, with Δt the hopping interaction whose physical origin is discussed in Ref. 21. U is the on-site Coulomb repulsion, D is the bandwidth, and ε_0 is the center of the band, defined by

$$\varepsilon_0=\frac{1}{N}\sum_k \varepsilon_k \tag{5}$$

with N the number of unit cells. Quite generally, one expects $U\gg V>\Delta t$. The critical temperature is determined by the equation

$$1+UI_0+WI_2+2KI_1-(K^2-WU)(I_0I_2-I_1^2)=0\ , \tag{6}$$

with

$$I_l=\frac{1}{N}\sum_k\left[-\frac{\varepsilon_k-\varepsilon_0}{D/2}\right]^l\frac{1-2f(\varepsilon_k-\mu)}{2(\varepsilon_k-\mu)}\quad l=0,1,2 \tag{7}$$

and μ the chemical potential. Below T_c, the gap function is

$$\Delta_k=\Delta_m\left[-\frac{\varepsilon_k-\varepsilon_0}{D/2}+c\right], \tag{8}$$

with Δ_m and c determined by Eq. (6) and

$$c=-K(I_2+cI_1)-U(I_1+cI_0)\ , \tag{9}$$

with $(\varepsilon_k-\mu)$ in Eq. (7) replaced by

$$E_k=\sqrt{(\varepsilon_k-\mu)^2+\Delta_k^2}\ . \tag{10}$$

We use the Slater-Koster Linear Combination of Atomic Orbitals method (SK-LCAO)[23] to calculate the band structures. The SK-LCAO parameters for nonorthogonal s, p, and d orbitals are tight-binding fits by Papaconstantopoulos[24] to first-principles-band structures. The two-center approximation was used and interactions up to the second nearest neighbors were included. The underlying band structure calculations do not include spin-orbit coupling.

To calculate the densities of states, we diagonalize the Hamiltonian for a large number of k points and calculate the densities of states $D(\varepsilon)$ by a histogram technique directly from the eigenvalues,

$$D(\varepsilon)=\frac{1}{N}\left[\sum_{\varepsilon-\delta\varepsilon/2\le\varepsilon_k<\varepsilon+\delta\varepsilon/2}1\right]/\delta\varepsilon\ . \tag{11}$$

For a given number of N_{mesh}, which is the number of k points along the symmetry axes, $\delta\varepsilon$ is estimated as the following:

$$\delta k\sim\frac{2\pi}{N_{\text{mesh}}a}\ , \tag{12}$$

$$\delta\varepsilon\sim\frac{\hbar^2(\delta k)^2}{2m_e}=\left[\frac{2\pi}{N_{\text{mesh}}}\right]^2\frac{\hbar^2}{2m_ea^2}\sim\left[\frac{2\pi}{N_{\text{mesh}}}\right]^2\text{ in rydberg}\ . \tag{13}$$

Here a is the lattice constant and m_e is the electron mass. By estimating $\delta\varepsilon$ in this way, we can avoid unphysical peaks in the density of states caused by too fine energy resolution.

For bcc materials, we diagonalize 9×9 Hamiltonian matrix for a uniform mesh of 45 526 k points (with $N_{\text{mesh}}=100$) in the irreducible 1/48th of the Brillouin zone. For fcc materials, we diagonalize 9×9 Hamiltonian matrix for a uniform mesh of 89 076 k points (with $N_{\text{mesh}}=100$) in the irreducible 1/48th of the Brillouin zone. For hcp materials, which have two atoms per unit cell, we diagonalize 18×18 Hamiltonian matrix for a uniform mesh of 18 081 k points (with $N_{\text{mesh}}=80$) in the irreducible 1/24th of the hexagonal Brillouin zone.

Since the experimental results use the number of valence electrons as a parameter instead of Fermi energy, we calculate the number of electron/atom at Fermi level ε_F as the following:

$$n=\frac{2}{N}\sum_{\substack{\text{all}\\ \text{bands}}}\sum_{k,\varepsilon_k\le\varepsilon_F}1\ . \tag{14}$$

To give a quantitative description of whether or not the Fermi level is at the top of a band, we define the number of unoccupied states of ith band as

$$n_h(i)=1-\frac{1}{N}\sum_{\substack{k,\varepsilon_k\le\varepsilon_F\\ i\text{th band}}}1\ . \tag{15}$$

The crystal structure of transition metals in group 5 and group 6 of the periodic table are mostly bcc, those in the adjoining groups 3,4 and 6,7 are mostly hcp, and those in groups 9 and 10 are fcc. It is established by experiments that the bcc region extends from 4.2 up to 6.5 electrons per atom. Elements in the same column have similar band structures and properties except for the magnetic metals in the 3*d* series. Since elements in the 4*d* series are lighter than those in the 5*d* series and their band structures are relatively well studied, we choose the 4*d* series as the focus of our investigation. Solid solutions of neighboring transition metals are believed to be well described by the band structure corresponding to the component with the same lattice structure as the alloy, and the Fermi level determined by the alloy concentration, i.e., the value of $e/a\equiv n$ in alloy A_xB_{1-x} is

$$n(A_xB_{1-x})=xN_e(A)+(1-x)N_e(B)\ , \tag{16}$$

with $N_e(A)$ and $N_e(B)$ the number of valence electrons in atoms A and B.

For the bcc region in the 4*d* series, Nb and Mo are two pure elements with bcc structure. We use molybdenum's band structure as the rigid band for the entire bcc region. For alloys with the hcp structure we use zirconium's band structure for n between 3 and 4.2, and technetium's band structure for n between 6.5 to 8.3. For n in the neighborhood of 9 (fcc structure) we use rhodium's band structure as the rigid band.

The total density of states across the 4*d* transition-metal series is shown in Fig. 1 for $3\le n\le 10$. We also show the measured transition temperatures.[25] Although some correlation exists between the two peaks in T_c and peaks in the density of states, the fact that superconductivity does not exist at the beginning and the end of the series cannot be correlated with the behavior of the density of states.

III. CALCULATION OF TRANSITION TEMPERATURES

We divide our study into three sections corresponding to the different lattice structures indicated in Fig. 1.

A. bcc region, $4.2\le n\le 6.5$

We consider for definiteness the band structure of molybdenum, $n=6$. Figure 2 shows the partial densities of states in each band as a function of n. It also indicates the boundaries of the bcc region, as well as the positions of Nb and Mo. It can be seen that the Fermi level of Nb lies near the top of the band labeled 2, while the Fermi level of Mo is approaching the top of the band labeled 3.

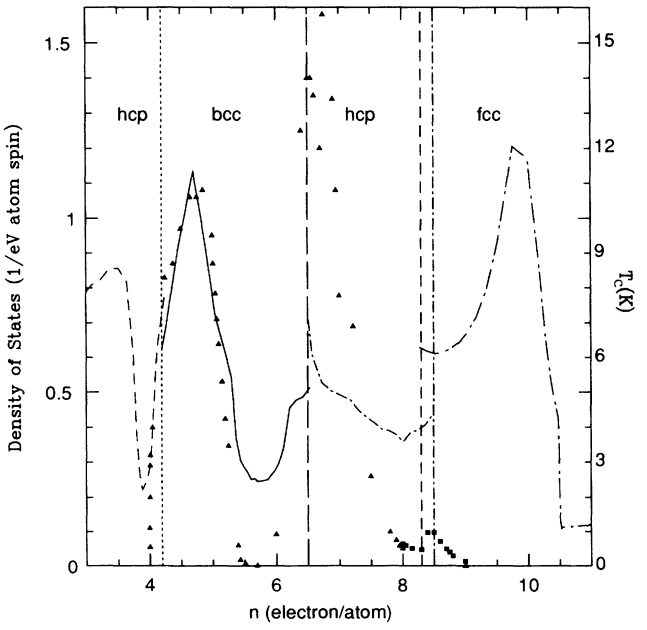

FIG. 1. Density of states vs electron per atom in the 4*d* transition-metal series. For $3\le n\le 4.2$, Zr's band structure is used as the rigid band; for $4.2\le n\le 6.5$, Mo's band structure is used; for $6.5<n\le 8.3$, Tc's band structure is used; for $8.5\le n\le 10$, Rh's band structure is used. Solid triangles are experimental data from 4*d* series; solid squares are those from 5*d* series (right scale).

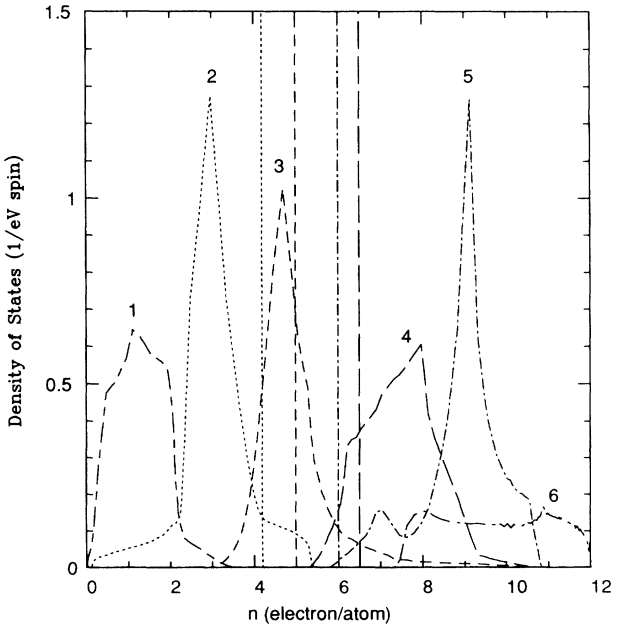

FIG. 2. The density of states of each band of molybdenum vs electron concentration. Vertical dotted line indicates the Fermi level at $n=4.2$; vertical short-dashed line is the Fermi level of Nb; vertical dot-dashed line is the Fermi level of Mo; vertical long-dashed line indicates the Fermi level at $n=6.5$.

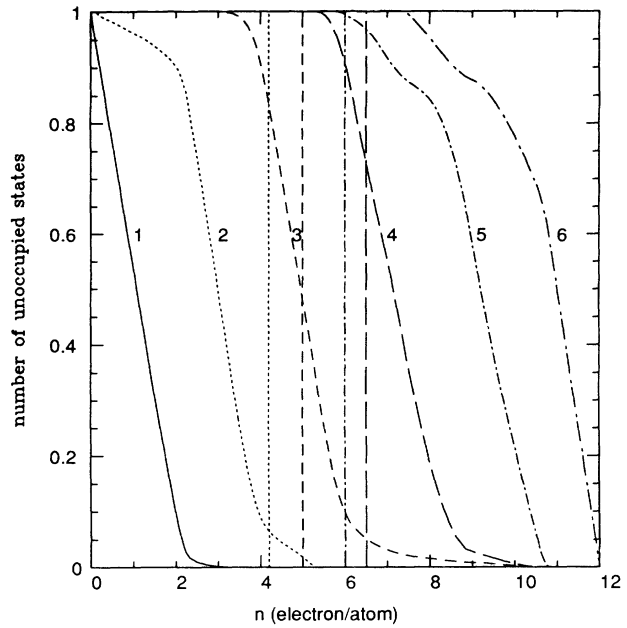

FIG. 3. The electron concentration dependence of the number of unoccupied states for each band of molybdenum. The center of each band $\varepsilon_0(i)$, $i=1,6$ corresponds to $n=0.996$, 2.993, 5.298, 7.046, 9.331, 11.016, respectively. The vertical lines are for the Fermi levels as indicated in Fig. 2.

We attribute the portion of the two peaks in T_c in the bcc region to carriers near the top of these two bands, respectively. For a clearer picture, Fig. 3 shows the number of unoccupied states in each band versus n. The onset of T_c in the second peak corresponds to having approximately 0.1 unoccupied states in band 3. For the first peak, at the stability boundary of the bcc phase, the number of unoccupied states in band 2 is approximately 0.06, and correspondingly, the observed T_c is appreciable.

For a quantitative fit we explored various sets of pa-

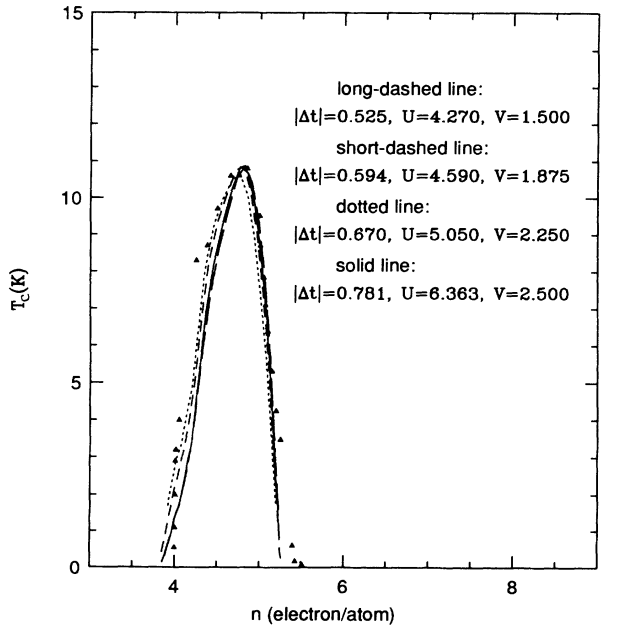

FIG. 4. The dependence of T_c on electron concentration for several sets of parameters for band 2 of Mo. Interactions are in units of eV.

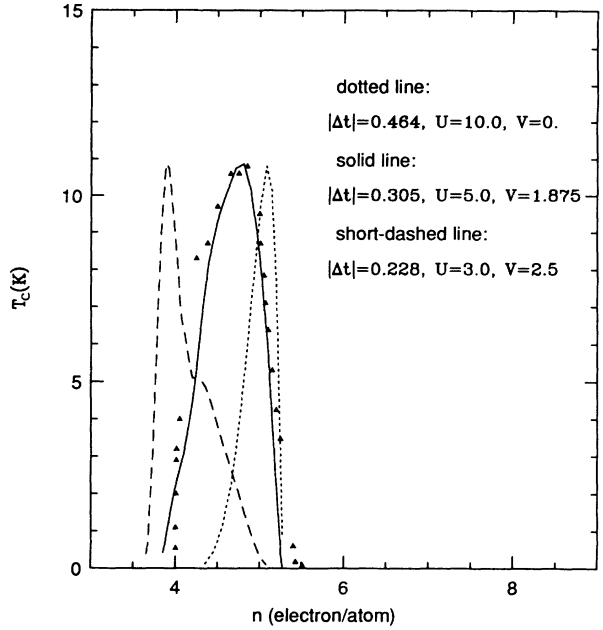

FIG. 5. The dependence of T_c on electron concentration for several sets of parameters for band 2 of Mo. Interactions are in units of eV.

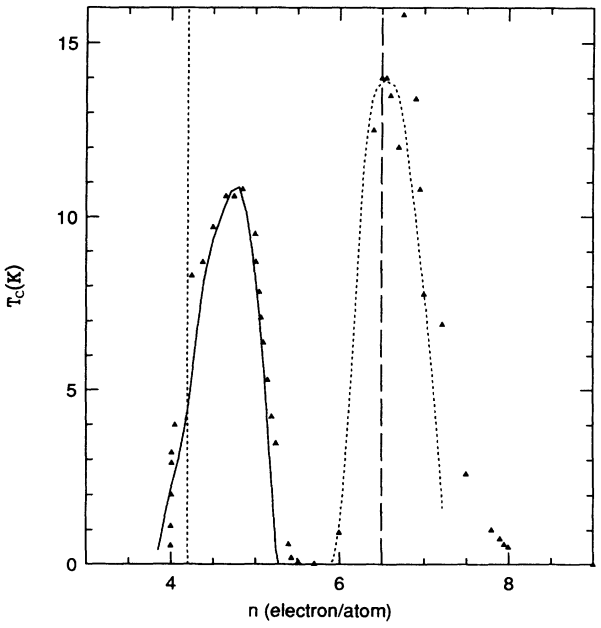

FIG. 6. The fit to experiments in the bcc region from the second and third bands of molybdenum. Solid line from second band, $U=4.590$ eV, $|\Delta t|=0.594$ eV, $V=1.875$ eV. Dotted line from third band, $U=8.0$ eV, $|\Delta t|=0.850$ eV, $V=1.875$ eV. The vertical lines indicate the boundary of the bcc region.

rameters in Eq. (4). For different parameters chosen to fit the position and height of the first peak, its width turned out to be approximately constant and in agreement with experiment as shown in Fig. 4. On the other hand, on changing the parameters so that the position of the peak would shift (with constant height), the width and shape of it would also change, as shown in Fig. 5 (the width decreases as the peak moves to higher n). Thus we regard the fact that the model can approximately fit the observed width, position, and height of the peak as significant. Figure 6 shows a possible fit to the two peaks within the bcc structure, using bands 2 and 3 of Mo. The interactions in band 3 are somewhat larger than in band 2, which may originate in the fact that the wave functions are becoming more compact. Figure 6 also shows the expected behavior of T_c, if one was able to stabilize the bcc structure beyond the currently attainable region, within the rigid band assumption.

Our model predicts no superconductivity in the region where band 2 is full and band 3 has more than about 0.1 holes per atom, i.e., $5.3 \leq n \leq 5.85$. However, experimentally a small T_c (of order mK) is found in this region. A possible explanation for this discrepancy may lie beyond the rigid band model. Qualitatively, in a Nb-rich region of such a Nb-Mo alloy some unoccupied states may exist near the top of band 2, giving rise to "negative U centers"[26] that may induce superconductivity in the entire system. In addition, the top of band 2 of Nb corresponds to slightly higher n values than Mo. A comparison of the densities of states in bands 2 and 3 of Nb and Mo is shown in Fig. 7.

Within a model that included electron-phonon interactions as well as the mechanism considered here,[27] one might also explore the possibility that the above-mentioned discrepancy could be resolved for sufficiently large electron-phonon coupling. This is, however, not within the scope of this paper.

B. hcp regions

In the lower hcp region, $3 \leq n \leq 4.2$, we use zirconium's band structure as the rigid band. Figure 8 shows the partial densities of states for each band, and Fig. 9 the integrated densities of states. We note at the outset that for $n = 3$, the Fermi level does not lie close to the top of any band; band 3, the closest to being full, still has 0.16 unoccupied states per atom. As we approach $n = 4$, the Fermi level approaches both the top of bands 3 and 4. Because of the larger density of states in band 4, for equal interactions, band 4 will dominate the superconducting behavior. The experimental data can be fitted in this region as shown in Fig. 10. For definiteness, we chose the nearest neighbor repulsion $V = 1.875$ eV, the same as in the bcc region. The other parameters are given in the figure caption.

In the upper hcp region in the transition-metal series we use technetium's band structure for the rigid band. Figures 11 and 12 show the partial and integrated densities of states, respectively. The Fermi level lies close to the top of bands 6 and 7 in the region of interest here ($6.5 \leq n \leq 8.3$). Figure 10 shows the behavior of T_c obtained from these two bands, with parameters given in the caption. It does not seem possible to fit T_c with our model using independent bands in this region, since we obtain a minimum around $n = 7.25$ which is not seen experimentally.

To explain the smooth behavior of T_c vs n in this re-

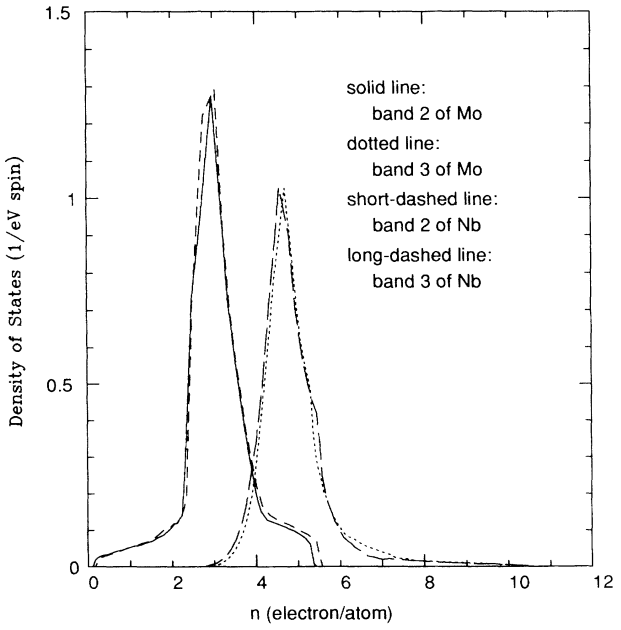

FIG. 7. The densities of states of the second and third bands of Nb and Mo.

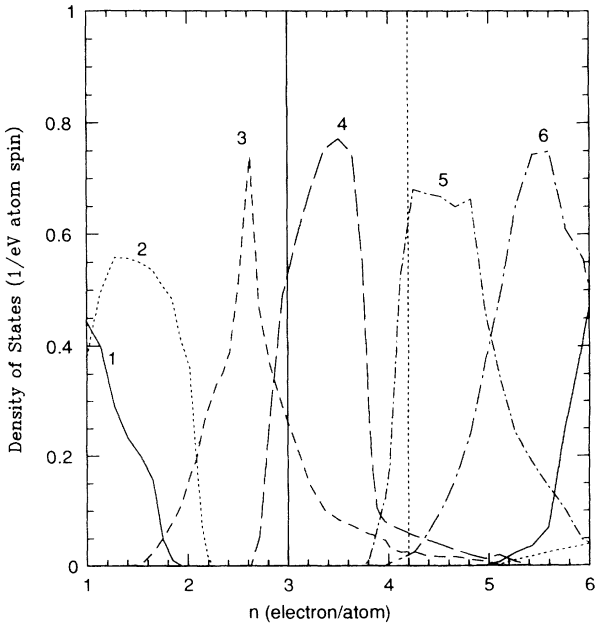

FIG. 8. The density of states of each band of zirconium vs electron concentration. Vertical solid line indicates $n = 3$; vertical dotted line indicates $n = 4.2$.

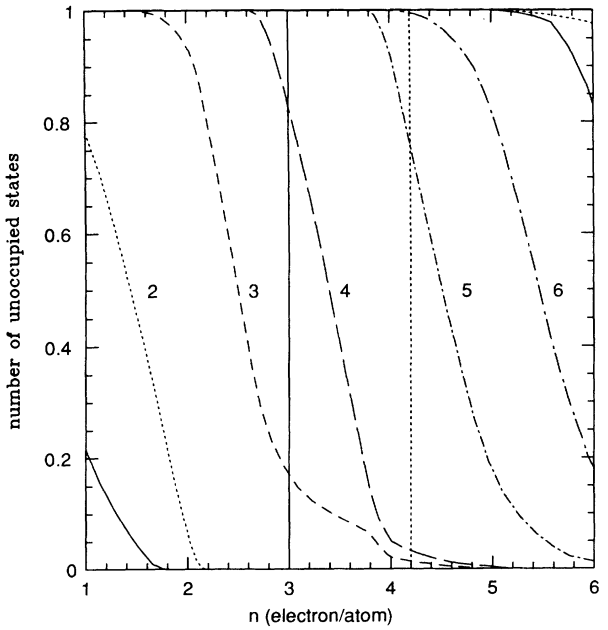

FIG. 9. The dependence of the number of unoccupied states for each band of zirconium on electron concentration. The center of first six bands $\varepsilon_0(i)$, $i=1,6$ corresponds to $n=0.328$, 1.414, 2.515, 3.473, 4.545, 5.501, respectively. Vertical solid line indicates $n=3$; vertical dotted line indicates $n=4.2$.

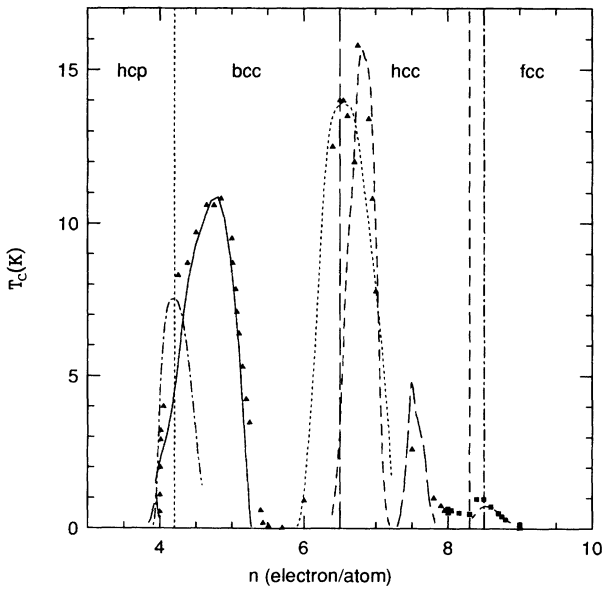

FIG. 10. The fit to experiments. Solid line from second band of Mo, $U=4.50$ eV, $|\Delta t|=0.594$ eV, $V=1.875$ eV. Dotted line from third band of Mo, $U=8.0$ eV, $|\Delta t|=0.850$ eV, $V=1.875$ eV. Short-dash-dotted line from band 4 of Zr, $U=10.0$ eV, $|\Delta t|=0.866$ eV, $V=1.875$ eV. Long-dash-dotted line from band 3 of Zr, with interactions same as band 4 of Zr. Short-dashed line from band 6 of Tc, $U=4.20$ eV, $|\Delta t|=0.563$ eV, $V=1.875$ eV. Long-dashed line from band 7 of Tc with same interactions as band 6. Short dash-long dash line from band 4 of Rh, $U=4.79$ eV, $|\Delta t|=0.563$ eV, $V=1.875$ eV. The region $8.3<n<8.5$ is a mixture of hcp and fcc.

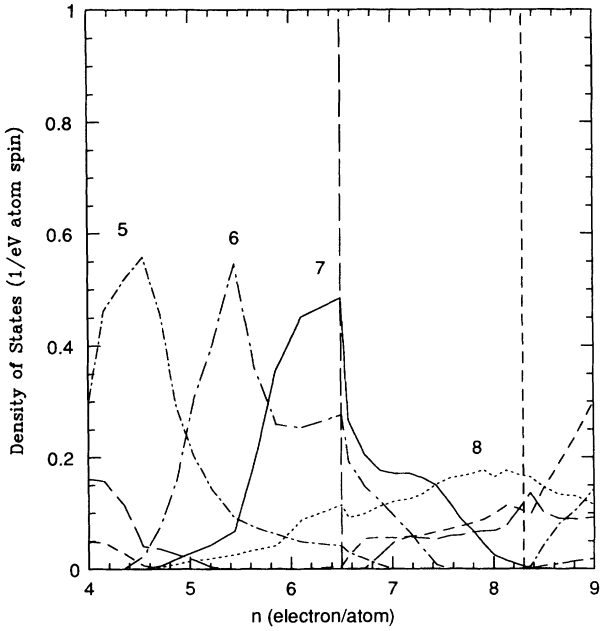

FIG. 11. The density of states of each band of technetium vs electron concentration. Vertical long-dashed line indicates $n=6.5$; vertical short-dashed line indicates $n=8.3$.

gion within our model, it is necessary to include interband scattering. It is possible that this effect may be generally important when there is more than one band with holelike carriers at the Fermi surface. Figure 13 shows the effect of including an interband term of the form in-

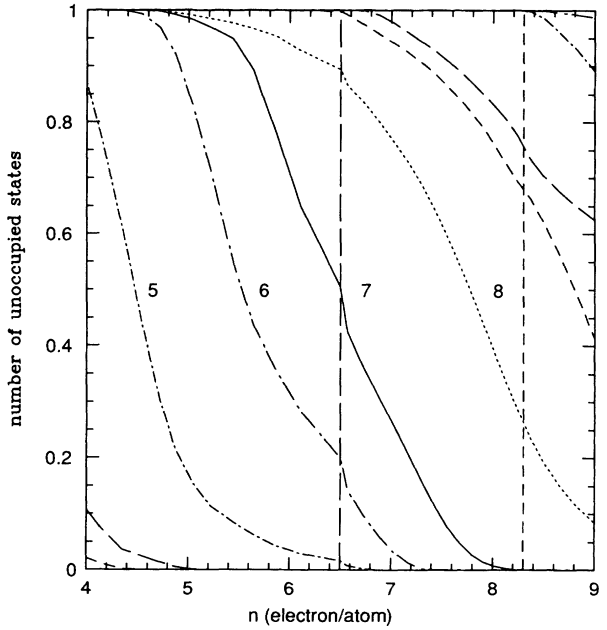

FIG. 12. The dependence of the number of unoccupied states for each band of technetium on electron concentration. The center of first ten bands $\varepsilon_0(i)$, $i=1,10$ corresponds to $n=0.439$, 1.445, 2.683, 3.441, 4.582, 5.721, 6.663, 7.791, 8.566, 9.045, respectively. Vertical long-dashed line indicates $n=6.5$; vertical short-dashed line indicates $n=8.3$.

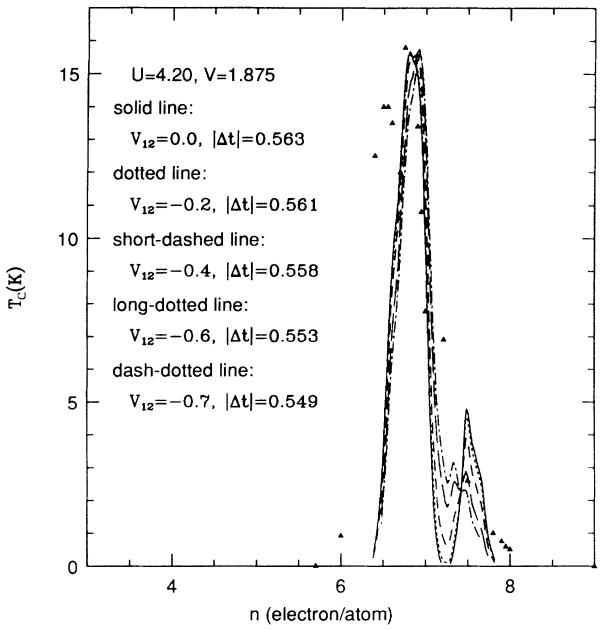

FIG. 13. The dependence of T_c on electron concentration when interband coupling exists between band 6 and band 7 of technetium. The interactions in the two bands are the same, $U_1=U_2=U(\Delta t)_1=(\Delta t)_2=\Delta t, V_1=V_2=V$. U and V are fixed, Δt is changed with V_{12} to keep T_c in same range. Interactions are in units of eV.

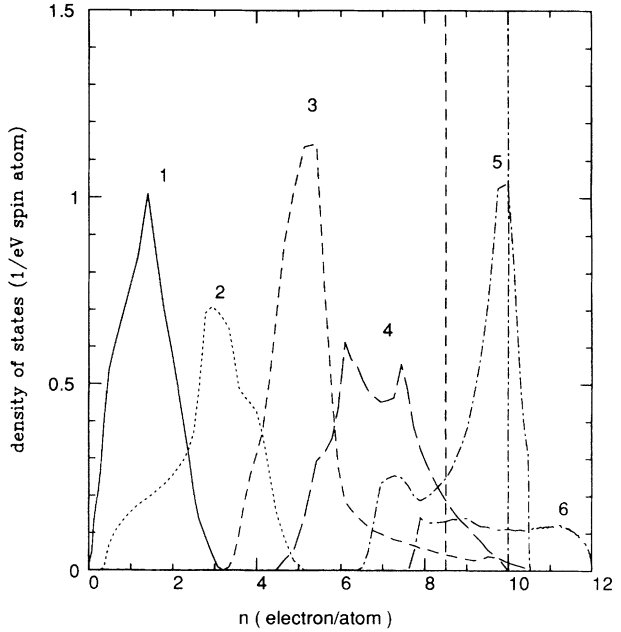

FIG. 14. The density of states of each band of rhodium vs electron concentration. Vertical short-dashed line indicates $n=8.5$; vertical dash-dotted line indicates $n=10$.

troduced by Suhl *et al.*,[28,29] coupling bands 6 and 7. It can be seen that the structure is smoothened and more closely resembles experimental observations.

It should also be mentioned that even better agreement with experiment in this region would be found by allowing the interactions in the model to change slightly with n, which would not be an unreasonable assumption due to the dependence of screening effects on electron density. Finally, the same remark made at the end of Sec. III A applies here.

C. fcc region

In the region $n>8$ the crystal structure becomes fcc and we use the tight-binding parameters of Rh ($n=9$) for our rigid band. Figures 14 and 15 show the partial and integrated densities of states. Band 4 of Rh is nearly full and has the largest density of states in the region around $n=9$, so that we use it to fit experimental values for T_c, as shown in Fig. 16. The experimental data are for the 5*d* series, as we were unable to find equivalent results for the 4*d* series. For $n=9$ our calculated T_c value is smaller than the observed value in the 5*d* series (Ir, $T_c=0.14$ K) but larger than the corresponding value in the 4*d* series (Rh, $T_c=0.0003$ K). As n increases beyond 9, band 4 becomes full and T_c goes to zero.

For $n=10$ (Pd), band 5 has still approximately 0.2 holes per atom which is usually too large a hole concentration to give rise to superconductivity in our model. However, if the interaction parameters used for band 4 are used in band 5, a nonzero T_c is obtained for Pd due to its very large density of states. One may speculate that the repulsive interactions may be larger in Pd because of the more compact nature of the electronic wave functions. In fact it has been argued that Pd is close to a

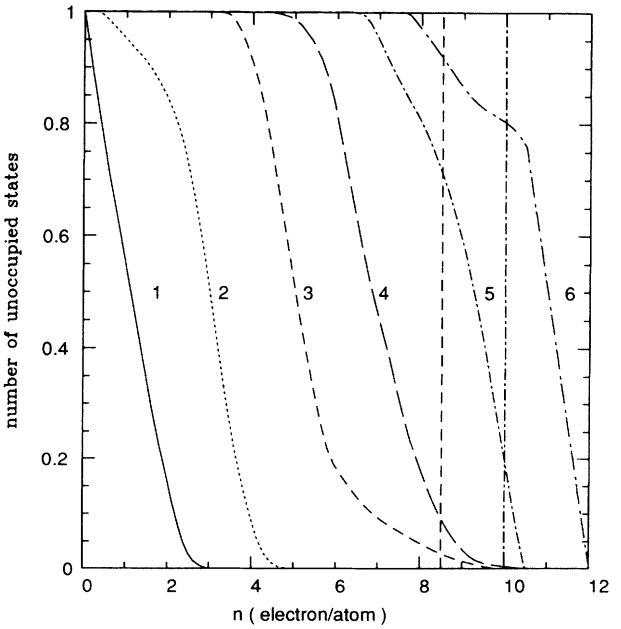

FIG. 15. The dependence of the number of unoccupied states for each band of rhodium on electron concentration. The center of first five bands $\varepsilon_0(i)$ $i=1,5$ corresponds to $n=0.996$, 2.924, 5.432, 6.971, 8.911, respectively. Vertical short-dashed line indicates $n=8.5$; vertical dash-dotted line indicates $n=10$.

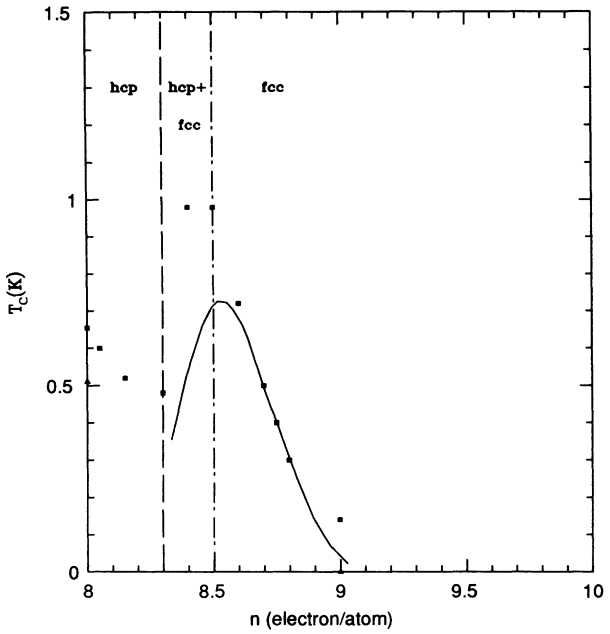

FIG. 16. The fit to experiments in the fcc region from the fourth band of rhodium, $U=4.79$ eV, $|\Delta t|=0.563$ eV, $V=1.875$ eV. Solid triangles are experimental data of $4d$ series. Solid squares are experimental data of $5d$ series.

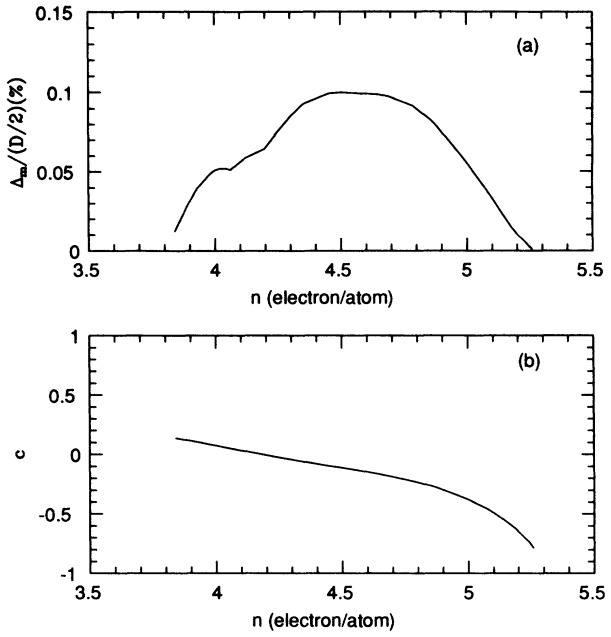

FIG. 17. Dependence of gap parameters on electron concentration in the bcc region from the second band in the bcc structure. (a) $\Delta_m/(D/2)\%$ vs n. (b) c vs n.

magnetic instability,[14] as evidenced by the large value of its magnetic susceptibility. If we use the same values of V and Δt as in band 4 but increase the value of U from 4.79 to 5.2 eV, no superconductivity is found for Pd (nor elsewhere in band 5) within our model.

IV. THE SUPERCONDUCTING STATE

In this section we examine some properties of the superconducting state within this model in the region of the first peak in T_c vs n, within the bcc structure. The behavior in the region of the second peak is expected to be very similar. Because the system is in the weak-coupling regime, only small deviations from "conventional" BCS behavior can occur.

The gap obtained from Eq. (8) is isotropic, i.e., constant over the Fermi surface, because pairing arises from a kinetic process in this model. To our knowledge, measured gaps in these systems are generally found to be remarkably isotropic.[30] Although this is usually explained as arising from the averaging effect of disorder, our model provides an alternative explanation for this observation.

The behavior of the parameters Δ_m and c in the gap function [Eq. (8)] versus n is shown in Fig. 17, and Fig. 18 shows the gap function versus energy for several n values. The fact that the gap function changes sign for energies near the bottom of the band allows for the existence of superconductivity with purely repulsive interactions, as discussed in Ref. 20: the larger repulsive interaction in the energy region of negative gap function results in a net attraction at low energies. The parameter c [Fig. 17(b)] determines the point at which the gap function changes sign: as n decreases, this point moves to higher energies while the chemical potential decreases; when this point coincides with the chemical potential, T_c goes to zero.

The parameter Δ_m [Fig. 17(a)] gives the slope of the gap function. As discussed in Ref. 31, the quantity

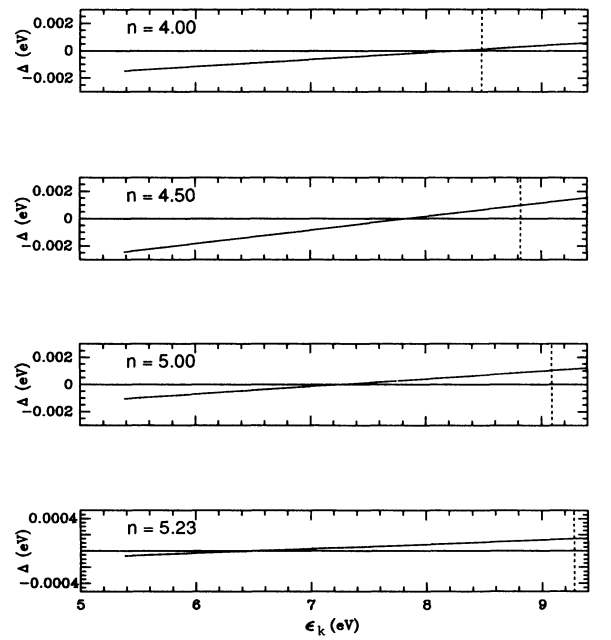

FIG. 18. Gap function vs energy for different electron concentration. Vertical dotted lines indicate the position of the Fermi level.

$[2\Delta_m/(D/2)]$ gives the fractional asymmetry in tunneling characteristics, i.e., the excess tunneling current in a negatively versus a positively biased sample. Unfortunately, as seen in Fig. 17, its magnitude is rather small in this case (maximum 0.2%) and thus difficult to detect experimentally.

The quasiparticle gap in this model is given by

$$\Delta_0=\frac{\Delta_k(\varepsilon_k=\mu)}{\sqrt{1+[\Delta_m/(D/2)]^2}} . \tag{17}$$

The gap ratio $2\Delta_0/k_BT_c$ is found to be given by the BCS value 3.53 except for a very small increase for large values of n (the largest deviation from the BCS value found, as T_c approaches zero in the upper part of the peak, is approximately 0.1%). This is in contrast to the behavior found in the parameter regime appropriate to high-T_c oxides, where the gap ratio can take values substantially larger than the BCS value near the top of the T_c vs n curve.[20]

We compute the coherence length ξ_0 from the average size of the pair wave function[20]

$$\xi_0=\frac{2\sqrt{2}}{\pi}\langle R^2\rangle^{1/2} , \tag{18a}$$

$$\langle R^2\rangle=\frac{\sum_R|f(R)|^2R^2}{\sum_R|f(R)|^2} , \tag{18b}$$

$$f(R)=\frac{1}{N}\sum_a\frac{\Delta_k}{2E_k}[1-2f(\varepsilon_k)]e^{i.k.R} . \tag{18c}$$

Equation (18b) can be written as

$$\langle R^2\rangle=\frac{\int d\varepsilon\, D_2(\varepsilon)|\frac{d}{d\varepsilon}\frac{\Delta(\varepsilon)}{2E(\varepsilon)}|^2}{\int d\varepsilon\, D(\varepsilon)|\frac{\Delta(\varepsilon)}{2E(\varepsilon)}|^2} , \tag{19}$$

with $D(\varepsilon)$ the density of states and

$$D_2(\varepsilon)=\frac{1}{N}\sum_k|\tilde{\nabla}_k\varepsilon_k|^2\delta(\varepsilon-\varepsilon_k) , \tag{20}$$

the average velocity. Within weak-coupling BCS theory, $\xi_0=\hbar v_F/\pi\Delta$, with v_F the Fermi velocity and Δ the energy gap.

Figure 19 shows the average velocities versus n for the different bands. Consistent with the calculation of T_c, we will only use the carriers in the second band for the calculation of the coherence length. Note that in the upper region of the first T_c peak ($n\geq 5$), the Fermi velocity in the second band is substantially smaller than in the third band. Thus our model predicts smaller "intrinsic" coherence lengths in this region than a BCS model that uses the average Fermi velocity in all bands.

The estimated[32] coherence length in Nb is approximately 430 Å. This rather small value of the coherence length results in Nb being a type-II rather than a type-I superconductor ($H_{c2}=0.4$ T, $H_c=0.2$ T). The inferred Fermi velocity in weak-coupling BCS (using $\Delta=1.44$ meV) is $v_F=0.30\times10^8$ cm/sec. The average Fermi velocity from Fig. 19 for $n=5$ is $v_F=0.54\times10^8$ cm/sec,

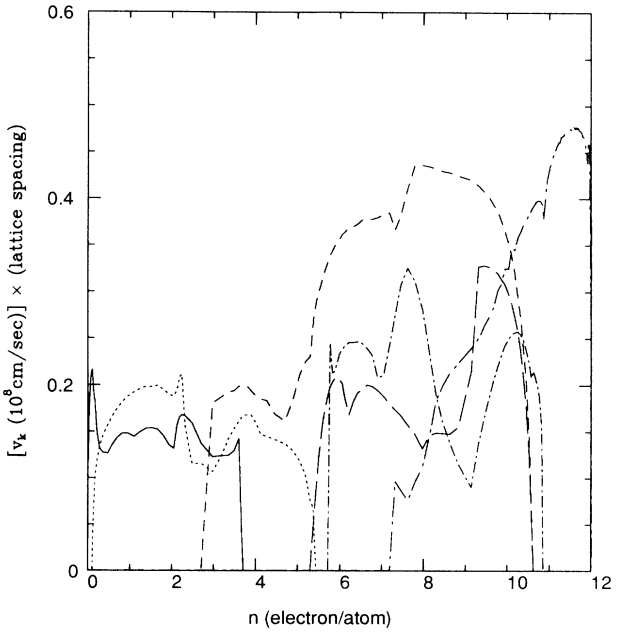

FIG. 19. Average velocity at Fermi energy [Eq. (20)] for each band in the bcc structure vs electron concentration.

while the Fermi velocity for carriers in the second band is 0.41×10^8 cm/sec. While both estimates yield too large a value for the coherence length, the estimate from band 2 is somewhat closer to the expected value. The actual coherence length obtained in our model from Eq. (18) is shown in Fig. 20 as a function of n. For Nb the value obtained is 190 lattice spacings, which is similar to the es-

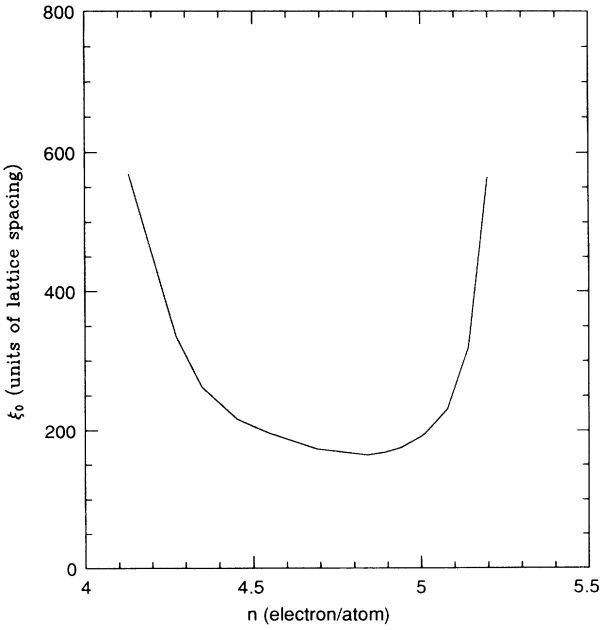

FIG. 20. Dependence of coherence length on the electron concentration in the bcc region from the second band in the bcc structure. The parameters are from Fig. 6, $U=4.590$ eV, $|\Delta t|=0.594$ eV, $V=1.875$ eV.

timate given by the BCS expression. Thus, while our result is better than that which would be obtained with the average Fermi velocity in all bands, it is still somewhat too large, for reasons unclear to us.

The coherence length shown in Fig. 20 qualitatively follows the behavior of the inverse critical temperature (as in conventional BCS theory), unlike the behavior found in the parameter regime of high-T_c oxides, where ξ was found to monotonically decrease with increasing n. This is because the parameter regime in this paper corresponds to a weak-coupling regime. For comparison with experiment, it should be kept in mind that the observed coherence length is affected by the amount of disorder in the sample.[33]

The mechanism discussed here leads to an apparent violation of the conductivity sum rule,[34] due to the gain in kinetic energy that occurs when the system enters the superconducting state. The contribution to the kinetic energy from the hopping interaction is given (for a bcc lattice) by

$$T_\delta^{\Delta t} = -\frac{K}{2}\Delta_m^2 (I_1 + cI_0)(I_2 + cI_1) , \tag{21a}$$

while the kinetic energy from the usual single-particle hopping process is

$$T_\delta^t = \frac{1}{2}\int d\varepsilon\, g(\varepsilon)(\varepsilon - \varepsilon_0) f(\varepsilon - \mu) \tag{21b}$$

and the degree of violation of the sum rule at low frequencies (i.e., associated with intraband processes) is given by the ratio of Eqs. (21a) and (21b). Unfortunately, due to the smallness of the parameter Δ_m [Fig. 17(a)], we find that this effect should be less than 0.1% in the parameter regime discussed here. Nevertheless, it is possible that either this or the associated resulting change in high-frequency optical properties[34] could be observable.

V. DISCUSSION

We have explored the possibility of describing superconductivity in the transition-metal series within the model of hole superconductivity. Our findings are summarized as follows.

First, there exist parameters in the model that appear to be plausible and can reproduce the observed behavior of T_c. It should be stressed that the value of T_c in this model is very sensitive to the magnitude of the parameters and we have no way at this point to estimate these parameters from first principles to the needed accuracy. Nevertheless, the model constrains quite strongly the possible values for T_c; for example, we have seen that the first peak in T_c can be fitted by several sets of parameters, but it would not be possible to fit a peak of the same height and width that was shifted from the position of the observed one. For all regions where superconductivity occurs in the transition-metal series it was possible to associate this fact with the Fermi level being located near the top of some band, as required by the model, and to fit T_c quantitatively with appropriately chosen parameters.

Furthermore, we have found that no superconductivity would be expected in our model near the third column in the periodic table (Sc,Y) due to the fact that the Fermi level is not located near the top of any band. In the band closest to being full (band 3 in Fig. 9), the number of holes in the third column is approximately 0.16, too large to give rise to superconductivity. It is possible that under application of pressure, electrons are transferred from band 4 to band 3, giving rise to a nonzero T_c as observed in Y under pressure.[25]

At the end of the transition-metal series, $n=10$ (Pd,Pt), we have seen that the Fermi level approaches the top of a band but is still rather far from it for $n=10$ (number of holes is 0.2), consistent with the absence of superconductivity in these metals with plausible values of interaction parameters. Unfortunately, to explain the observed absence of superconductivity beyond $n=10$ (e.g., in Pd-Ag or Pt-Au alloys[35]) one has to invoke the existence of large Coulomb repulsion, as is done in studies using the electron-phonon interaction.[14] Without this additional assumption, our model in fact would suggest that superconductivity should exist beyond $n=10$ as the upper d band becomes filled, contrary to observations. It is interesting to note, however, that the measured Hall coefficients in both Pd,Pt as well as in Sc and Y are negative,[36] unlike in the other transition metals.

Note that the fact that the two observed peaks in T_c in the transition-metal series correlate with peaks in the density of states[4] is accidental within our model. (Also within the conventional theory, the magnitude of the coupling constant is believed to dominate T_c far more than a peak in the density of states at the Fermi level.) For example, in the cubic region we have seen that the two peaks in T_c originate in holes in the second and third bands in Fig. 2, respectively. Instead, the peaks in the density of states originate dominantly in the contributions from bands 3 and 4, respectively. It is seen in Sec. IV that some evidence in favor of the hypothesis that it is band 2 rather than 3 that gives rise to superconductivity in Nb, is the observed smallness of the coherence length ξ_0, which suggests a dominant role for the carriers in band 2 that have a smaller Fermi velocity.

We have also explored some properties of the superconducting state within this model. The slope in the gap function (Fig. 18) is what allows for the existence of superconductivity with purely repulsive interactions. Unfortunately, the slope was found to be so small that it may be difficult to obtain direct evidence for it in tunneling experiments. Also, no appreciable deviation from the weak-coupling BCS gap ratio was found. The predicted violation of the conductivity sum rule within this model and associated change in high-frequency optical properties[34] should similarly give rise to only a very small effect in this parameter range. Thus it would appear to be difficult to find direct experimental support for our model in the parameter regime appropriate to the transition-metal series, and one may have to look at other systems such as high-T_c oxides or possibly $A15$'s for clearer signatures. It is important to point out, however, that our model could be easily *ruled out* in this or any other regime, by finding a superconductor that clearly does not have hole states at the Fermi energy.

It is also interesting to note that our model may pro-

vide an alternative explanation to McMillan's observation[5] that the largest T_c's correspond to smallest values of the denominator in Eq. (3). As the Fermi level approaches the top of a band, antibonding states become increasingly occupied and one expects the lattice to become increasingly unstable, i.e., "soft." This correlation was pointed out by Varma and Dynes.[37]

We regard the fact that the model discussed here can reproduce the observed values of T_c in the transition-metal series with plausible parameters as encouraging. While the present study certainly does not prove that the model describes superconductivity in the transition-metal series, we believe it suggests that further studies of this model are warranted as a possible alternative to the electron-phonon model.

ACKNOWLEDGMENTS

This work was supported by NSF-DMR-8918306. We are grateful to D. A. Papaconstantopoulos for making available to us his computer codes for the computation of the tight-binding band structures. Computations were performed at the San Diego Supercomputer Center.

[1]B. T. Matthias, in *Progress in Low Temperature Physics,* edited by J. C. Gorter (North Holland, Amsterdam, 1957), Vol. 2, p. 138.

[2]J. K. Hulm and R. D. Blaugher, Phys. Rev. **123**, 1569 (1961).

[3]For a review, see S. V. Vonsovsky, Y. A. Izyumov, and E. Z. Kurmaev, *Superconductivity of Transition Metals* (Springer, Berlin, 1982).

[4]D. Pines, Phys. Rev. **109**, 280 (1958).

[5]W. L. McMillan, Phys. Rev. **167**, 331 (1968).

[6]J. J. Hopfield, Phys. Rev. **186**, 443 (1969).

[7]D. A. Papaconstantopoulos *et al.*, Phys. Rev. B **15**, 4221 (1977).

[8]I. R. Gomersell and B. L. Gyorffy, Phys. Rev. Lett. **33**, 1286 (1974).

[9]J. C. Carbotte and R. C. Dynes, Phys. Rev. **172**, 476 (1968).

[10]P. B. Allen and M. L. Cohen, Phys. Rev. **187**, 525 (1969).

[11]B. A. Sanborn, P. B. Allen, and D. A. Papaconstantopoulos, Phys. Rev. B **40**, 6037 (1989).

[12]See, however, the discussion by D. Rainer, Physica **109&110B**, 1671 (1982).

[13]A. Y. Liu and M. L. Cohen, Phys. Rev. B **44**, 9678 (1991).

[14]G. Gladstone, M. A. Jensen, and J. R. Schrieffer, in *Superconductivity,* edited by R. D. Parks (Marcel Dekker, New York, 1969), Vol. II, p. 665.

[15]J. Bostock *et al.*, Phys. Rev. Lett. **36**, 603 (1976); also in *Superconductivity in d- and f-band Metals,* edited by H. Suhl and M. B. Maple (Academic, New York, 1980), p. 153.

[16]R. C. Dynes (private communication).

[17]J. G. Bednorz and K. A. Muller, Z. Phys. B **64**, 189 (1986).

[18]I. M. Chapnik, Dok. Akad. Nauk SSSR **6**, 70 (1962) [Sov. Phys. Dokl. **6**, 988 (1962)]; Phys. Lett. **72A**, 255 (1979); J. Phys. F **13**, 975 (1983); Phys. Status Solidi B **123**, K183 (1984).

[19]A. Lightman and O. Gingerich, Science **255**, 690 (1992).

[20]J. E. Hirsch and F. Marsiglio, Phys. Rev. B **39**, 11 515 (1989); F. Marsiglio and J. E. Hirsch, Phys. Rev. B **41**, 6435 (1990); Physica C **165**, 71 (1990).

[21]J. E. Hirsch, Phys. Lett. A **134**, 451 (1989); Physica C **158**, 326 (1989); Chem. Phys. Lett. **171**, 161 (1990); Phys. Rev. B **43**, 11 400 (1991); J. E. Hirsch and S. Tang, Phys. Rev. B **40**, 2179 (1989).

[22]A preliminary discussion of the application of this model to the transition-metal series was presented in J. E. Hirsch and F. Marsiglio, Phys. Lett. A **140**, 122 (1989); further details of this work can be found in X. Q. Hong, Ph.D. thesis, University of California, San Diego, 1992.

[23]J. C. Slater and G. F. Koster, Phys. Rev. **94**, 1498 (1954).

[24]D. A. Papaconstantopoulos, *Handbook of the Band Structure of Elemental Solids* (Plenum, New York, 1986).

[25]B. W. Roberts, J. Phys. Chem. Ref. Data **5**, 581 (1976).

[26]H. B. Schuttler, M. Jarrell, and D. J. Scalapino, Phys. Rev. Lett. **58**, 1147 (1987).

[27]F. Marsiglio, Physica C **160**, 305 (1989).

[28]H. Suhl, B. T. Matthias, and L. R. Walker, Phys. Rev. Lett. **3**, 552 (1959).

[29]X. Q. Hong and J. E. Hirsch, Phys. Rev. B **45**, 12 556 (1992).

[30]V. Z. Kresin and S. A. Wolf, *Fundamentals of Superconductivity* (Plenum, New York, 1990).

[31]F. Marsiglio and J. E. Hirsch, Physica C **159**, 157 (1989).

[32]D. K. Finnemore, T. F. Stromberg, and C. A. Swenson, Phys. Rev. **149**, 231 (1966).

[33]M. Tinkham, *Introduction to Superconductivity* (McGraw-Hill, New York, 1975).

[34]J. E. Hirsch, Physica C **199**, 305 (1992); **201**, 347 (1992).

[35]B. T. Matthias, Phys. Rev. **92**, 874 (1953); F. E. Hoare and B. Yates, Proc. R. Soc. London Ser. A **240**, 42 (1957); D. W. Budworth, F. E. Hoare, and J. Preston, *ibid.* **257**, 250 (1960).

[36]C. M. Hurd, *The Hall Effect in Metals and Alloys* (Plenum, New York, 1972).

[37]C. M. Varma and R. C. Dynes, in *Superconductivity in d- and f-band Metals,* edited by D. M. Douglass (Plenum, New York, 1976), p. 507.